High-throughput phenotyping of physiological traits for wheat resilience to high temperature and drought stress

Pedro M. P. Correia[1]*, Jesper Cairo Westergaard[2], Anabela Bernardes da Silva[1], Thomas Roitsch[2,3], Elizabete Carmo-Silva[4], Jorge Marques da Silva[1]

[1] BioISI – Biosystems & Integrative Sciences Institute, Faculdade de Ciências da Universidade de Lisboa, Campo Grande, 1749-016 Lisboa, Portugal

[2] Department of Plant and Environmental Sciences, Section of Crop Science, Copenhagen University, Højbakkegård Allé 13, 2630 Tåstrup, Denmark

[3] Department of Adaptive Biotechnologies, Global Change Research Institute, CAS, 603 00 Brno, Czech Republic

[4] Lancaster Environment Centre, Lancaster University, Library Avenue, Lancaster, LA1 4YQ, UK

* To whom correspondence may be addressed. Email: pmpcorreia@fc.ul.pt

Date of submission: 31/10/2021

Word count: 3683

Number of Manuscript Pages: 29

Total Number of Figures: 8

Total Number of Tables: 1

Supplementary data: 3 Figures, 3 Tables

Running Title: Wheat high-throughput phenotyping high temperature and drought

Highlight

High-throughput phenotyping highlighted the importance of canopy architecture to fine-tune transpiration. The interplay between sucrolytic and glycolytic pathways is essential to tolerate drought at high temperature in wheat.

Abstract

Interannual and local fluctuations in wheat crop yield are majorly explained by abiotic constraints. Heatwaves and drought, which are among the top stressors, commonly co-occur, and their frequency is increasing with global climate change. High-throughput methods were optimised to phenotype wheat plants under controlled water deficit and high temperature, with the aim to identify phenotypic traits conferring adaptative stress responses. Wheat plants of 10 genotypes were grown in a fully automated plant facility under 25/18ºC day/night for 30 days, and then the temperature was increased for seven days (38/31ºC day/night) while maintaining half of the plants well irrigated and half at 30% field capacity. Thermal and multispectral images and pot weights were registered twice daily. At the end of the experiment, key metabolites and enzyme activities from the carbohydrate and antioxidant metabolisms were quantified. Regression machine learning models were successfully established to predict plant biomass using image-extracted parameters. Evapotranspiration traits expressed significant genotype-environment interactions (GxE) when acclimatization to stress was continuously monitored. Consequently, transpiration efficiency was essential to maintain the balance between water-saving strategies and biomass production in wheat under water deficit and high temperature. Stress tolerance included changes in the carbohydrate metabolism, particularly in the sucrolytic and glycolytic pathways, and in the antioxidant metabolism. The observed genetic differences in sensitivity to high temperature and water deficit can be exploited in breeding programs to improve wheat resilience to climate change.

Keywords: Carbohydrate metabolism, climate change, drought resilience, food security, high temperature, high-throughput plant phenotyping, multispectral imaging, *Triticum aestivum*, water deficit, wheat.

Introduction

Wheat is a major staple food in numerous regions worldwide (FAOSTAT, 2019). Around 40% of the global wheat yield fluctuations are explained by environmental constraints, being heatwaves and drought among the top stressors (Deryng *et al.*, 2014; Zampieri *et al.*, 2017). Moreover, several wheat-growing regions are characterized by hot and dry summers, where drought is likely to coincide with elevated temperatures more frequently in the future (Araus, 2002; Russo *et al.*, 2018). Understanding the interaction between drought and high temperature on crop production is challenging, as simultaneous stresses may have additive, synergistic or antagonistic effects on plants' physiology (Rizhsky *et al.*, 2004; Tricker *et al.*, 2018). Furthermore, such response integrates several phenological and physiological processes under multigenic controls, and depends on the individual sensitivity to the microenvironment (Parent *et al.*, 2017). As a result, continuous monitoring of plants response to controlled stress conditions is essential to understand plant-environment interactions. High-throughput phenotyping methods appeared as the solution to compensate the otherwise labour-intensive and time-consuming classic methods of systematic plant phenotyping (Fiorani and Schurr, 2013; Fahlgren *et al.*, 2015; Tardieu *et al.*, 2017; Roitsch *et al.*, 2019).

Crop production is intimately dependent on carbon uptake by photosynthesis, and stomatal opening is vital for carbon capture. However, in response to water shortage, higher plants close stomata to limit water losses by transpiration (Chaves *et al.*, 2003; Nunes *et al.*, 2009; Duque *et al.*, 2013) and when subjected to high temperatures, plants usually use evaporative cooling to reduce leaf temperature, which could otherwise be detrimental to several physiological processes (Carmo-Silva *et al.*, 2012; Costa *et al.*, 2013; Lawson *et al.*, 2018). An optimal balance between risk avoidance and performance is critical to crop production under water deficit and high-temperature conditions (Tardieu, 2012; Moshelion, 2020). When photosynthetic performance and plant growth are challenged by water shortage and elevated temperatures, remobilization of the carbohydrate metabolism through adjustment of source-sink relations is crucial to tolerate stress and accelerate recovery to reduce yield fluctuations (El Habti *et al.*, 2020; Correia *et al.*, 2021).

Several carbohydrate metabolism enzymes demonstrated fundamental functions in drought stress tolerance (Albacete *et al.*, 2011, 2015; Pinheiro and Chaves, 2011; Secchi and Zwieniecki, 2016; Antonio Cuesta-Seijo *et al.*, 2019; Shokat *et al.*, 2020), although little is known about their role in drought at high temperature. Furthermore, stress exposure usually leads to excessive accumulation of reactive oxygen species (ROS), causing damage to plasma membranes, proteins and pigments, and if the capacity of scavenging and repairing mechanisms is exceeded, photosynthesis and crop performance are constrained (Foyer and Noctor 2005; Tricker et al. 2018). Antioxidant capacity was associated with tolerance to drought or heat stress in wheat (Sairam *et al.*, 2000; Lascano *et al.*, 2001; Zhang *et al.*, 2017), although the importance of ROS scavenging, both enzymatically and/or by the production of several antioxidant compounds, in combined stresses is unknown.

In this study, we continuously monitored biomass allocation, plant-water relations and reflective properties in ten genotypes with heterogeneous performance under water deficit and high temperature conditions. Including some of the best available elite advanced lines (check lines), selected based on their superior performance and verified in multi-year yield trials at the International Maize and Wheat Improvement

Center (CIMMYT) breeding site (Reynolds et al., 2017). Physiological Trait lines (PT lines), the outline of a breeding strategy where crosses were designed to complement "source" (biomass) with "sink" traits (harvest-index, kernel weight, grains per spike) (Reynolds *et al.*, 2017) and parental lines used for trait-based crossing (Reynolds *et al.*, 2007; Manès *et al.*, 2012). The contrasting levels of tolerance to drought and heat of the ten wheat genotypes were explored to (1) optimize high-throughput methods to phenotype wheat plants under drought and high temperature; (2) profile the plant-water-environment relationship of each genotype under these conditions; (3) understand the regulatory mechanisms of the primary carbohydrate and antioxidant metabolisms associated with plants' response to drought at high temperature. The effects of long-term (7 day) growth under high temperature (WW38) and water deficit at high temperature (WD38) on traits related to leaf reflectance proprieties, water use, and biomass accumulation were assessed in a high-throughput phenotyping station and linked to the carbohydrate and antioxidant metabolism regulation.

Materials and Methods

Germplasm and growth conditions

Ten spring wheat (*Triticum aestivum* L.) genotypes were selected based on their heterogeneous performance under water deficit or high temperature conditions (Table 4.1). BORLAUG, SOKOLL and BAJ are check lines; PASTOR and SOKWB_1 were included in the Stress Adapted Trait Yield Nurseries trial (SATYN, CIMMYT) and highly performed in drought-stressed areas (SATYN series with odd numbers); PUBWB and SOKWB_2 showed outstanding performance in SATYN under heat stress conditions (SATYN series with even numbers); CMH82 and KSPA are parental lines; PARAGON is a traditional UK spring wheat elite cultivar (Moore, 2015; Pennacchi *et al.*, 2019), with good tolerance to water deficit and high temperature when characterized alongside SOKOLL (Correia *et al.*, 2021).

Plants were grown from seeds for 15 days (DAS 15) in 1 L well-watered pots containing horticultural substrate (SW Horto AB, Hammenhög) plus 10% perlite in a greenhouse at 25/18℃ (day/night), 50% relative humidity (RH) and a photoperiod of 16 hours. Plants were then moved to the phenotyping greenhouse (PhenoLab, PLEN UCPH), automated for plant care and movement, with the same climatic conditions and well-watered (WW >90% field capacity). After 15 days (30 DAS), the temperature was changed to 38/31ºC (day/night), and the plants were randomly assigned to two different irrigation treatments: five plants per cultivar were maintained WW (WW38), and five plants were subject to water deficit (WD38) for seven days. WD was established by withholding watering and sustaining a minimum of 30% field capacity. The soil water content was determined gravimetrically by automatically weighing the pots twice a day, and irrigation was provided to compensate for evapotranspiration and keep the soil water content in the WW and WD pots. Pots containing only soil were maintained at the same watering regime and weighed to estimate non-transpirational water loss under WW38 and WD38 treatments. Leaf samples for biochemical analyses were collected at the end of the experiment (DAS 37), 5-7 h after the beginning of the photoperiod, frozen into liquid nitrogen and stored at -80°C.

High-throughput data acquisition and extraction

Multispectral images were automatically acquired by a top-mountedCCD camera (PhenoLab, Videometer) twice a day from 15 to 37 DAS. A hemisphere setup (PhenoLab, Videometer) was used to assure homogeneous and diffuse illumination of the plants by high power narrow banded LEDs at ten discrete spectral bands (365, 460, 525, 570, 645, 670, 700, 780, 890, 970 nm). Thermography was obtained using a thermal camera (Flir A65, FLIR Systems Inc.). Multispectral images consisting of stacked photos, each with a specific spectral band, were analysed via a supervised classification method (normalized Canonical Discriminant Analysis, nCDA) in the software VideometerLab (version 3.0.33, Videometer). Based on this procedure, crop coverage (plant exposed area) was automatically calculated from segmented transformed images and pixel reflectance intensities extracted from the same region of interest (ROI). Thermographic data extraction was automated by using masks from the segmentation of multispectral images. In the software MATLAB (version r2019a, The MathWorks Inc.) the multispectral image was geometrically transformed by image registration to the thermal image. The resulting transformation file was used for automated transformation of all the multispectral masks to fit the geometry of the thermal images, allowing for segmentation of the thermal signal from each acquisition of the plant parts and calculation of the temperature statistics. Evapotranspiration was calculated from the gravimetric data obtained at the irrigation time as the water loss per hour between consecutive measurements (mg H_2O h^{-1}). As all the pots in each treatment were in the same conditions (soil, capacity, and water availability), randomly distributed, automatically reorganized (four times daily), and measured twice a day, differences in evapotranspiration between them can be attributed to variations in plant transpiration.

Plant harvesting and biomass prediction

At the end of the experiment (37 DAS), plants were harvested to measure aboveground and roots fresh weight (FW) and dry weight (DW). Roots were separated from the soil by manual washing with water, and shoots were harvested by cutting immediately above ground level. FW was directly measured on an electronic scale, and DW was measured after oven drying samples at 70°C for 52 h. Architectural traits as the number of leaves and tillers was also assessed before harvesting. Predictive models were constructed based on sixteen machine-learning regression methods implemented in the predMod module of the HTPmod Shiny application (Chen *et al.*, 2018*a*) and tested to predict plant biomass (FW and DW) from image-extracted features (37 DAS), as applied in Chen et al. (2018b). A 10-fold cross-validation strategy was adopted to check the prediction power of each regression model. The dataset was randomly divided into a training set (70% of plants) and a testing set (30% of plants). The trained model, based on the training data, was then applied to predict biomass for the testing set of plants. Models were considered for further application if the following criteria for the prediction performance were satisfied: (1) Pearson correlation coefficient of determination (R^2) between the predicted values and the observed values >0.7; (2) root mean squared relative error of cross-validation (MRSRE) <0.3; (3) predictive bias between the predicted and observed values (μ) <0.05. A Linear Support Vector Machine model (svm-linear, *caret* R package (Kuhn, 2008) was then used to predict FW and DW from 15 until 37 DAS from image-derived features.

Growth modelling

Ten different mechanistic models implemented in the growMod module of the HTPmod Shiny application (Chen *et al.*, 2018*a*) were tested to model plant growth and applied as described in Chen et al. (2014). Models were considered if the following criteria for the fitting quality were satisfied: (1) R^2>0.7; (2) P<0.05. The time point of maximum biomass (Timemax), maximum final vegetative biomass (biomass at Timemax) , were extracted from the models.

Intrinsic growth rate (GR), which measures the speed of growth, was estimated as:

$$1.\ \mathrm{GR} = \ln(\text{Biomass at Timemax} - \text{Biomass at T1}) / (\text{Timemax} - \text{T1}),$$

where T1 is the time point of stress imposition (30 DAS).

The water use efficiency (WUE) from 30 to 37 DAS of each plant, corresponding to the biomass produced per water transpirated, was calculated as:

$$2.\ \mathrm{WUE} = (\text{Biomass at Timemax} - \text{Biomass at T1})/(\text{Timemax } \mathrm{H_2O} - \mathrm{T1H_2O}),$$

where T1H2O is the total water supplied at the time point of stress imposition, Timemax H2O is the total water supplied at Timemax, excluding the non-transpirational water loss (water loss in pots only with soil under the same irrigation regime). Comparison of plant growth between WW38 and WD38 conditions was assessed through a number of specific stress tolerance indices (Fischer and Maurer, 1978; Bouslama and Schapaugh, 1984; Grzesiak *et al.*, 2012) calculated with the parameters extracted from the growth models:

$$3.\ \text{Mean productivity} = (\text{Biomass at Timemax}_{\mathrm{WW38}} + \text{Biomass at Timemax}_{\mathrm{WD38}})/2;$$

$$4.\ \text{Biomass reduction} = \text{Biomass at Timemax}_{\mathrm{WD38}} / \text{Biomass at Timemax}_{\mathrm{WW38}};$$

$$5.\ \text{Inflection point stability} = \text{Timemax}_{\mathrm{WW38}} - \text{Timemax}_{\mathrm{WD38}}.$$

$$6.\ \mathrm{GR\ ratio} = \mathrm{GR}_{\mathrm{WD38}} / \mathrm{GR}_{\mathrm{WW38}};$$

$$7.\ \mathrm{WUE\ ratio} = \mathrm{WUE}_{\mathrm{WD38}} / \mathrm{WUE}_{\mathrm{WW38}};$$

Enzymes extraction

Frozen wheat leaf samples were homogenized in liquid nitrogen with 1% (w/v) insoluble polyvinylpyrrolidone (PVP). Total protein was extracted from samples (0.5 g FW) in ice-cold extraction medium containing 40 mM TRIS-HCl pH 7.6, 3 mM $MgCl_2$, 1 mM ethylenediaminetetraacetic acid (EDTA), 0.1 mM phenylmethylsulfonyl fluoride (PMSF), 1 mM benzamidine, 14 mM β-mercaptoethanol, 24 µM nicotinamide adenine dinucleotide phosphate ($NADP^+$), following the protocol described in Jammer et al. (2015). Total soluble protein (TSP) content was determined according to the Bradford method (Bradford, 1976) using BSA Fraction V as standard protein. Extracts were aliquoted, frozen in liquid nitrogen and stored at -20°C.

Activity of carbohydrate metabolism enzymes

The activity of nine enzymes from the carbohydrate metabolism was measured in thawed leaf extracts using a semi-high-throughput protocol in 96-well microtiter plates as described in Jammer et al. (2015) with variable extract volume (1-5 µL), and monitoring absorbance at 30°C (ELx808, BioTek Instruments, Inc.).

Briefly, Aldolase (Ald, EC 4.1.2.13) and Phosphofructokinase (PFK, EC 2.7.1.11) activities were measured by coupling the reactions with a Glycerol-3-phosphate dehydrogenase (GPDH) NADH-dependent reaction and recording the decrease in absorbance at 340 nm due to conversion of NADH to NAD^+. ADP-glucose pyrophosphorylase (AGPase, EC 2.7.7.27), Glucose-6-phosphate dehydrogenase (G6PDH, EC 1.1.1.49), Hexokinase (HXK, EC 2.7.1.1), Phosphoglucoisomerase (PGI, EC 5.3.1.9) and Phosphoglucomutase (PGM, EC 5.4.2.2) activities were assayed by linking the reactions with a G6PDH NADP-dependent reaction and recording the increase in absorbance at 340 nm due to conversion of $NADP^+$ to NADPH. Cytoplasmic invertase (cytINV, EC 3.2.1.26) and vacuolar invertase (vacINV, EC 3.2.1.26) activities were measured in an end-point assay, and the amount of liberated glucose was determined by measurements of absorbance at 405 nm. All reactions were carried out in triplicates alongside control reactions (in the absence of substrate), and enzyme activity was expressed relative to the amount of TSP in each sample.

Quantification of carbohydrates

Carbohydrates were extracted from frozen leaf samples homogenized in liquid nitrogen (0.1 g FW) by homogenization in ethanol (80% v/v) for 5 minutes at 80ºC and then centrifuged at 20,000 *g* for 5 min. The supernatant was collected, allowed to evaporate overnight at 60ºC, diluted in dH_2O and used to quantify sucrose, glucose, and fructose by an enzymatic method (kit AK00201, NZYTech) in a miniaturized protocol in 96-well microtiter plates following the manufacturer recommendations. The pellet was used to quantify starch by the same method after acidic hydrolysis in 30% HCl (v/v) at 90℃ for 15min.

Activity of antioxidant enzymes

The activity of four enzymes from the antioxidant metabolism was measured in thawed samples using a semi-high-throughput protocol in 96-well microtiter plates as described in Fimognari et al. (2020), with variable extract volume (1-5 µL), by monitoring absorbance at 30°C (ELx808, BioTek Instruments, Inc.). Briefly, ascorbate peroxidase (APX, EC 1.11.1.11) activity was measured by recording oxidation of ascorbate at 290 nm. Catalase (CAT, EC 1.11.1.6) activity was assayed by recording the decomposition of H_2O_2 at 240 nm. Peroxidase (POX, EC 1.11.1.7) activity was measured by recording the formation of tetraguaiacol at 450 nm. Superoxide dismutase (SOD, EC 1.15.1.1) activity was measured by recording the inhibition of the oxidation of cytochrome c at 550 nm. All reactions were carried out in triplicates alongside control reactions (in the absence of substrate), and enzyme activity was expressed relative to the amount of TSP.

Quantification of antioxidant capacity and metabolites

Antioxidant metabolites were extracted from frozen leaf samples homogenized in liquid nitrogen (0.4 g FW) by homogenization in pure methanol overnight in the dark at 4ºC and then centrifuged at 20,000 *g* for 5 min. The supernatant was aliquoted and stored at -20°C. Antioxidant metabolites and capacities were quantified in thawed samples using a miniaturized protocol in 96-well microtiter plates and monitoring absorbance (Synergy HTX, BioTek Instruments Inc.). Trolox equivalents antioxidant capacity (TEAC) and ferric reducing antioxidant power (FRAP) were quantified as described in Correia et al. (2020). Total phenolic

content was determined by the Folin-Ciocalteu method (Singleton *et al.*, 1999) by recording the absorbance at 765 nm. Galic acid standards in ddH_2O were measured alongside the samples and used to prepare the respective calibration curves. The total phenolic content of the extract was expressed as mg Galic acid equivalents per gram of leaf (mg g^{-1} FW). The total flavonoids content was determined by the $AlCl_3$ method (Zhishen *et al.*, 1999) by recording the absorbance at 510 nm. Catechin was used as a standard for the calibration curve. The total flavonoids content of the extract was expressed as mg catechin equivalents per gram of sample (mg g^{-1} FW). Anthocyanins content was assessed by the pH-differential method (Giusti and Wrolstad, 2001) and expressed as cyanidin-3-glucoside equivalents (mg g^{-1} FW).

Data pre-processing and analysis

Traits extracted from the images and gravimetrical measurements were pre-processed for outlier detection, trait reproducibility and collinearity assessment using the same approach as Chen et al. (2014). Briefly, Grubbs' test (Grubbs, 1950) was used to detect outliers in replicated plants in each genotype at the same condition and data point, outliers were deleted and missing values were imputed (missForest R package, Stekhoven & Bühlmann, 2012). Traits were considered as highly reproducible if the following criteria were satisfied in at least one treatment condition: (1) the median correlation coefficient over genotypes was larger than 0.7; (2) the coefficients were significantly higher in replicates than in random plant pairs (Welch's t-test $P < 0.05$). To reduce the excessive correlation among explanatory variables (multicollinearity), a stepwise variable selection using variance inflation factors (VIFs) was applied, traits were considered if VIF < 5. The observed variance in phenotypic traits, enzymatic activities and metabolites amounts was partitioned into components attributable to different sources of variation, the variation of genotype (G), environment (E), and their interaction (GxE), using the same approach as Chen et al. (2014). Briefly, a linear model was applied to determine the likelihood of genotype-to-phenotypes linkage for each trait measured in each day, *P*-values were corrected for multiple comparisons with the Benjamini-Hochberg false discovery rate method (fdr), the LOD scores (log of odds) were calculated, as the -log probability (corrected *P*-value, fdr) (Joosen et al. 2013). A heat map representation and hierarchical clustering were applied to the matrix of LOD scores or tolerance indices. ANOVA and post-hoc comparison (Duncan test, $P < 0.05$) were also used to dissect the statistical significance of individual trait variation between genotypes. A t-test ($P < 0.05$) was used for comparison between two treatments (WD38 and WW38) within the same genotype. A partial least squares-discriminant analysis (PLS-DA) was performed to classify and discriminate plants into treatments (WW38, WD38) and genotypes for each treatment and to identify the key variables that drive such discrimination (MixOmics R package, Rohart et al., 2017).

Results

Phenotypic descriptors reflecting the response to water deficit and high temperature

Traits with low reproducibility and high collinearity were filtered and extracted from the data set to avoid redundant or low-quality descriptors of the ten wheat genotypes (Table 1). A total of 15 traits reflecting the

three trait classes were maintained (Fig. 1), two traits reflecting leaf temperature (LeafT), three traits associated with the evapotranspiration processes (Evap.), and ten traits reflecting the multispectral signature. The statistical significance on phenotypic variance (LOD score) was determined to identify the traits that could reflect an effect of the genotype (G), treatment (E, environment) and their interaction (GxE) for each measurement day. All traits, excepting LeafT, increased LOD scores for G effect when stress was imposed (30-32 DAS, Fig.1A and Table S1), but a gradual decrease of differences in multispectral traits was observed until the end of the experiment (37 DAS). Interestingly, at 30 DAS, it was possible to discriminate between different groups: check lines (BAJ, BORLAUG), PT lines (PASTOR, PUBWB, SOKWB_1, SOKWB_2) and the other genotypes (Fig. S1A-B). At 37 DAS, the genotypes' distribution was more uniform and centralised horizontally under WD38 (Fig. S1C) and vertically under WW38 (Fig. S1D). At this stage, most of the traits exhibited similar LOD scores (Fig.1A and Table S1). The Environment effect (E) altered thermal, evapotranspiration progressively after stress imposition (Fig. 1B and and Table S2). Although, a slower reaction was observed for LeafT that only changed after 31 DAS (Fig. 1B and Table S2). Multispectral traits showed a distinct dynamic after stress imposition (Fig. 1B and Table S2). No change was observed for UVA and Blue (365-460nm). On the other hand, green, yellow and reds (525-700 nm) decreased LOD sores, showing a similar behaviour in G effect, and NIR (700-970) LOD scores slightly increased after 35 DAS (Fig 1B and and Table S2). All traits were observed to have significant GxE effects when the temperature increased from 25 to 38ºC (30 DAS; Fig. 1C and Table S3). On the other hand, only the traits related to evapotranspiration expressed significant GxE differences until the end of the experiment (37 DAS), indicating a strong influence of high temperature and extended drought on genetic factors related to these traits.

Indicators of water status

Genotype-environment effects changed significantly the phenotypic variance of traits related to evapotranspiration over the period when plants were exposed to high temperature and water deficit. Daily evapotranspiration (Evap.daily) was explored in more detail to understand the relevance of these adjustments, generally related to the water status and transpiration efficiency. Evapotranspiration increased with temperature, although when plants were exposed to water deficit (WD38), water availability rapidly decreased and under these conditions evapotranspiration decreased after stress imposition in all genotypes (Fig. 2A-J). Only CMH82 (Fig. 2C), PARAGON (Fig. 2E) and SOKWB_1 (Fig. 2I) did not show a significant difference between treatments at 30 DAS. Under WD38 conditions (Fig. 2K), KSPA, PASTOR and SOKWB_2 showed low evapotranspiration, while BORLAUG100, CMH82, PARAGON and SOKOLL displayed high values. When only exposed to high temperatures (WW38, Fig. 2L), BAJ, BORLAUG, SOKOLL showed the highest values and CMH82, KSPA and SOKWB_1 the lowest. At the end of stress exposition (37 DAS, Fig. 2M-N) under WD38 conditions (Fig. 2M), KSPA, SOKOLL and SOKWB_1 showed low values of evapotranspiration, contrasting PUBWB and BORLAUG100 with high values. Under WW38 (Fig. 2N), KSPA showed low levels of evapotranspiration and PARAGON high levels (Fig. 2N).

Under WD38, a positive correlation between the ratio of evapotranspiration to aboveground biomass (Evap/AerialDW) and evapotranspiration was observed (Fig. 3A). Under WW38, aboveground biomass correlated positively with evapotranspiration (Fig. 3B).

Biomass prediction from images and plant growth modelling

Regression models were developed to quantify the ability of geometrical traits to predict the aboveground biomass (DW, FW), measured at 37 DAS, in order to investigate the relationship between the image-extracted parameters and plant biomass. From the sixteen tested machine-learning regression models implemented in predMod (Chen *et al.*, 2018*a*), nine passed the defined criteria for model selection: R^2 >0.7; MRSRE <0.3; μ <0.05 (Fig. 4). Linear Support Vector Machine (SVM-linear, in red) was selected as the best model due to the low predictive bias (μ) and similar results for the other parameters (Fig. 4).

The geometrical traits area exposed (area.low) and pyramidical plant volume (volumepyr, calculated from the area and plant height) showed high predictive power. Moreover, the model constructed with the two parameters showed slightly higher accuracy to predict DW and FW, under WD38 and WW38 conditions, compared to the best single trait model, only with area.low (Fig. 5). FW predicted with the SVM-linear regression model built with the data extracted from images taken over plant growth (area.low and volumepy) showed the best correlation to FW measured and concomitant correlation to DW (Fig. 5). As the predicted fresh biomass (FW_sv) showed a better correlation to the measured biomass (FW and DW) compared to the predicted dry biomass (DW_sv), FW_sv was used as a proxy of plant aboveground biomass to model plant growth from 15 DAS until the forecasted 41 DAS (Fig. 6).

To determine the best model for biomass accumulation in wheat plants subjected to WW38 and WD38, ten different mechanistic models implemented in growMod (Chen *et al.*, 2018*a*) were tested. A Bell shape model satisfied the previously established criteria (R^2>0.7, P<0.05) for all genotypes in WW38 and WD38 conditions, with the best fit (R^2) for all the genotypes under WD38 and comparable results to the logistic model in WW38, and was thus selected to represent plant growth (Fig. 6). Different dynamics were observed between genotypes and stress conditions. The maximum biomass prediction (Biomass at Timemax) under WW38 was extracted from the growth model of Sokoll at 37 DAS (23.5 g, Fig. 6H) and the lowest for CMH82 at 36 DAS (12.9 g, Fig. 6C). Under WD38, the highest value was observed in SOKWB_2 at 36 DAS (16.5 g, Fig. 6E) and the smallest in CMH82 at 35 DAS (12.7 g, Fig. 6C).

Tolerance indices revealing stress symptoms

To characterise and classify the genotypes according to their growth dynamics under WW38 and WD38, stress tolerance indices were calculated with the parameters extracted from the growth models and the genotypes clustered accordingly (Fig. 7). CMH82 showed a distinct behaviour with high biomass stability, low productivity, minor changes in GR between conditions and elevated WUE under WD38 (Fig. 6C and Fig. 7). KSPA and SOKWB_1 showed a premature inflection point (Timemax) under WD38 relative to WW38, the highest reduction in the GR and WUE ratio (Fig. 6D, I and Fig. 7). However, SOKWB_1 showed higher

productivity and biomass reduction, whereas KSPA was the only genotype with a higher WUE under WW38 than WD38 (Fig. 6D, I and Fig. 7). PARAGON and SOKOLL revealed the highest mean productivity (MP) and high biomass reduction (BRR), although PARAGON showed a less accentuated reduction of GR and higher WUE under WD38 (Fig. 6E and H and Fig. 7). BAJ, BORLAUG100, PASTOR and PUBWB demonstrated a similar behaviour with average values (Fig. 6 A,B,F,G and Fig. 7), the only emphasis was on the higher value of WUE in BORLAUG100, due to the elevated productivity and inflection point stability (Fig. 6B and Fig. 7). SOKWB_2 showed high MP, more akin to SOKWB_1 (Fig. 7). However, similarly to BAJ and BORLAUG100, it exhibited a high inflection point stability (Fig. 6H, A, B and Fig. 7).

Impact of WD38 and WW38 on phenotypic traits and adjustment of carbohydrate and antioxidant metabolism

Significance of variance associated with genotype (G), treatment (E) and their interaction was evaluated for phenotypic traits including the activity of key enzymes and metabolites from the carbohydrate and antioxidant metabolism to dissect the components relevant to the response to water deficit under high temperature. CAT, POX, cytINV, AGPase, vacINV activities, antioxidant capacities (TEAC and FRAP), phenols and starch content revealed the strongest G effects (Fig. 8A). On the other hand, anthocyanins, flavonoids, phenols, fructose content, vacINV, PFK activities, FRAP and the number of leaves displayed the highest environmental effects (Fig. 8A). CytINV, vacINV, HXK, PFK, Aldolase, AGPase, POX activities, TEAC, FRAP and phenols content expressed significant genotype-environment interactions (GxE) (Fig. 8A). The traits that expressed significant GxE differences at the end of the experiment were linked to the carbohydrate and antioxidant metabolism and were explored in more detail to understand the regulatory mechanisms linked to WD38 and WW38. Except for KSPA, PASTOR and SOKOLL, all the genotypes experienced changes in cytINV or vacINV activities. From those, only CMH82 demonstrated an increase of cytINV activity under WD38. PUBWB only showed significant differences in vacINV and SOKWB_2 in cytINV, despite the high activity under both conditions in cytINV and vacINV (Fig. 8B). CMH82 showed the strongest activity of HXK under WD38 concomitantly with significant changes in PARAGON and PUBWB. Excluding KSPA and BORLAUG100, all the other genotypes exhibited significantly higher activity under WW38. BORLAUG100, CMH82, KSPA, PASTOR, PUBWB, SOKOLL and SOKWB_2 demonstrated a significantly elevated activity of PFK under WD38. SOKOLL showed a robust activity of Aldolase under WD38, CMH82 exhibited differences in a minor scale, and KSPA revealed high intrinsic activity despite no differences between conditions. CMH82 showed elevated activity of AGPase under WD38, and to a lesser extent, BAJ, PARAGON and PUBWB showed a significantly higher activity under the same condition. On the other hand, significant increases in the antioxidant capacity and activity occur only under WD38 (Fig. 8C-D). BAJ, KSPA, PARAGON, SOKOLL and SOKWB_2 exhibited changes in all the traits. BORLAUG only showed differences in POX activity and SOKWB_1 in phenols amount (Fig. 8C-D).

Discussion

The impact of water deficit at high temperature on phenotypic traits related to reflectance proprieties, water use and biomass accumulation was assessed in ten spring wheat lines. The pool of genotypes with

heterogeneous performance to drought stress or high temperature conditions was used to investigate genetic and environmental interaction (GxE) of trait response in a phenotyping platform with a controlled high temperature and water regime. Additionally, to understand the regulatory mechanisms of the primary carbohydrate and antioxidant metabolisms associated with wheat response to drought at high temperature, the activities of key enzymes and metabolism associated with those pathways were analysed.

We identified an overall strong genotype reflectance signature throughout the experiment, which was intensified when temperature increased (30 DAS, Fig. 1A). This indicates constitutive differences in pigments/secondary metabolites and leaf structure between genotypes (Merzlyak *et al.*, 2003; Blackburn, 2007). On the other hand, only NIR intensities (700-970nm) were related to the response to water deficit (LOD scores increased after 35 DAS, Fig. 1B), consistently with the decrease of water content, as reported in previous drought experiments (Seelig *et al.*, 2008; Chen *et al.*, 2014; Junker *et al.*, 2015). Together, these results showed that spectrometric measurements are important tools to detect the early response to the increase of temperature and to sense the response to drought stress. However, in our experimental setup, it was not possible to discriminate the genotype response to the combination of high temperature and water deficit using only multispectral reflectance.

Moreover, genotype-environment effects significantly changed evapotranspiration throughout the response to high temperature and water deficit (Fig. 1C, 2, 3). At the end of the experiment under WD38, all the genotypes decreased evapotranspiration to 40% relative to WW38, however we could identify three distinct transpiration behaviours in face of water deficit at high temperature. While CMH82, PARAGON and SOKWB_1 maintained the same evapotranspiration rate throughout the WD38 treatment; BAJ, BORLAUG and SOKOL (check lines) decreased transpiration gradually upon stress imposition; and KSPA, PASTOR, PUBWB and SOKWB_2 decreased transpiration on the first day under WD38 (70% relatively to WW38), then maintained it stable for the following two days prior to a subsequent continuous decrease (Fig. 2). Additionally, the data establish a correlation under WD38 between evapotranspiration and transpiration efficiency (ratio between biomass and evapotranspiration) (Fig. 3A). On the other hand, evapotranspiration under WW38 was more related to aboveground biomass (Fig. 3B). Schoppach et al. (2016) also identified a trade-off between night and day transpiration and biomass in wheat response to high vapour pressure deficit (VPD). Other studies associated transpiration efficiency and increased yield potential in well-watered and water-limited environments to high stomatal densities and conductance (Roche 2015; Shahinnia et al. 2016). As water use is essential for either drought or heat tolerance, these results highlight the importance of the balance between evaporative cooling, water-saving and photosynthesis in wheat genotypes growing under water deficit and high temperature. Additionally, the results obtained in our experimental setup evidence that gravimetrical measurements are more accurate than thermal measurements in detecting differences in the water status of genotypes in response to water deficit at high temperatures.

Biomass accumulation is a major indicator of plant performance and a key trait in plant breeding, however, conventional approaches are labour and time consuming and plants need to be harvested and destroyed to measure biomass (Catchpole and Wheeler, 1992; Cobb *et al.*, 2013). Using imaging data and a Linear Support Vector Machine algorithm (SVM-linear) we could accurately estimate biomass accumulation under high temperature and the combination of high temperature and water deficit (Fig. 4-5). Furthermore,

mechanistic models to estimate plant biomass are systematically and accurately used to estimate plant growth dynamics (Woodward and Hunt, 1983; Meade *et al.*, 2013; Tessmer *et al.*, 2013; Chen *et al.*, 2014). Our results indicate that a Bell shape model is the best model to characterise wheat's growth dynamic under single heat stress and when combined with water deficit (Fig. 6). Chen *et al.*, (2014) also identified the bell-shaped model as the best model to describe the growth pattern of 18 barley genotypes in response to water deficit. The more accurate fit of this model, in contrast to a sigmoid model usually followed by plant growth under non-stressful conditions (Paine *et al.*, 2012; Tessmer *et al.*, 2013), can be explained by the more complex behaviour of those. Notably, plants under stressful conditions can undergo wilting, resulting in a decrease in volume. Accordingly, there was a higher correlation between FW and plant volume, as DW does not take into account changes in plant architecture due to water loss in the tissues. The decrease in FW and plant volume also increases the challenge of precise biomass prediction under water deficit. Future experiments including a greater number of destructive measurements of biomass will enable validation and improvement of plant growth prediction.

In this study, by the complementation of automatic non-invasive phenotypic measurements with robust methods for data extraction and analysis, we could characterize the complex and dynamic processes of wheat growth and water use (Fig. 7). Dissecting the growth dynamics and water use of the poll of wheat genotypes with divergent performance, we identified CMH82 as highly tolerant to WD38, however, this genotype also decreases the potential to biomass accumulation under WW38, showing the lowest WUE and the worst mean productivity in both conditions. This behaviour would be advantageous under prolonged high temperatures associated with very dry conditions, but most likely would have a negative effect under the more common agricultural conditions (Tardieu, 2012; Parent *et al.*, 2017). This tolerance mechanism was associated with a large modulation in the carbohydrate metabolism, with higher activity in most enzymes related to sucrolytic and glycolytic pathways (Fig. 8). If carbohydrates are used for glycolysis in the leaves, sink strength is lost in other organs, and it is most likely that assimilates will be less available for reproductive organs and grain filling, causing yield penalties (Shokat et al. 2020; Roitsch and González 2004). Nevertheless, CMH82 showed higher activity of cytINV under WD38, which was previously associated with a faster recovery from water deficit and high temperature (Correia *et al.*, 2021). On the other hand, KSPA showed high WUE under WW38 but high susceptibility to WD38, without major changes in the carbohydrate metabolism. These results suggest that modulation of the carbohydrate metabolism upon water deficit at high temperature can be regarded as an essential protective mechanism. Paragon showed the best trade-off between WUE efficiency under WD38/WW38 and biomass production, demonstrating tolerance to growth under high temperature and mid-water deficit generally experienced in field conditions. Most of the genotypes with high WUE under WD38 showed higher activity of HXK under this condition. HXK is responsible for the phosphorylation of hexoses, acting as a glucose sensor to interconnect nutrient, light, and hormone signalling networks for controlling growth in response to environmental variations (Moore *et al.*, 2003) and is associated with the acquisition of desiccation tolerance (Whittaker *et al.*, 2001). Almost all the genotypes demonstrated high activity of PFK related to the increase of glycolysis and reallocation of carbohydrates to respiration under WD38. The increase of cytINV and vacINV activities was also observed in leaves of barley exposed to high temperature (Antonio Cuesta-Seijo *et al.*, 2019), while tomato leaves exposed to water deficit demonstrated

lower activity of cytINV and vacINV (Albacete *et al.*, 2015). Likewise, hexoses accumulation was only observed in leaves under WD38 (Fig. S3), showing that besides the increase of the sucrolytic activity under WW38, carbohydrates are being remobilized to other tissues.

Concerning the antioxidant enzymes evaluated, POX showed the highest genotype-environment effect, and although the different genotypes demonstrated different levels of activity, all of them increased POX activity under WD38. These results highlight the importance of POX activity in oxygen peroxide (H_2O_2) scavenging under water deficit and high temperature, resulting in better control of ROS levels and protection against oxidative damage. Other studies also highlighted the importance of the modulation of peroxidases activities to ROS scavenging under drought and high temperature (Koussevitzky *et al.*, 2008; Zandalinas *et al.*, 2017). ROS detoxification under WD38 was also associated with a non-enzymatic antioxidant defence, demonstrated by the increase of antioxidant capacity (FRAP and TEAC) and production of phenolic compounds.

In summary, this study illustrates the importance of canopy architecture to fine-tune transpiration required to achieve an equilibrium between water-saving, leaf evaporative cooling and biomass production when water deficit occurs at high temperature. Furthermore, it highlights the importance of transpiration efficiency to the maintenance of water uptake and transpiration/photosynthesis under these circumstances. The application of this methodology in further experiments connecting anatomical (number/size of stomata), phenological (number, shape, and angle of leaves), and functional traits (stomatal conductance and transpiration rate) to stress tolerance will help to elucidate the role of each component in the adaptation to fluctuations in water deficit associated to high temperature. Furthermore, our results highlighted the importance of adjustments in the carbohydrate and antioxidant metabolism to tolerate these stressful conditions, more specifically in the sucrolytic (cytINV), glycolytic pathways (HXK, PFK), and the ROS scavenging by POX and phenolic compounds. The integration of cell physiological phenotyping, via the semi-high-throughput determination of enzyme activity signatures and metabolites, with high-throughput phenotyping methods, proved to be an efficient approach to quantitatively characterize genotype-environment interaction of these complex traits. Further experiments with higher replication and collection of samples to quantify enzyme activity signatures/metabolites and biomass in a different phenological stage can further help to prove the robustness of the provided approach and results. The application of this methodology into breeding programs will facilitate the selection of promising candidates for wheat production in environments subjected to high temperatures and drought.

Author contributions

Pedro M. P. Correia planned and carried out the experiments, analysed and interpreted the results. Jesper C. Westergaard extracted the data from thermal and multispectral images. Elizabete Carmo-Silva and Jorge Marques da Silva contributed to the interpretation of the results and supervised the research. Anabela Bernardes da Silva and Thomas Roitsch provided critical feedback. Pedro M. P. Correia took the lead in writing the manuscript. All authors discussed the results and contributed to the final manuscript.

Data Availability Statement

All data supporting the findings of this study are available within the paper and within its supplementary materials published online. Further inquiries can be directed to the corresponding author (Pedro M.P. Correia), upon request.

Acknowledgments

We would like to thank Gemma Molero (CIMMYT) for the supply of wheat seeds and Rene Hvidberg Petersen for help with plant growth.

Funding

The reported work was carried out within the project EPPN2020 for which funding was received from the European Union's Horizon 2020 research and innovation programme under grant agreement No 731013. The financial support provided by UIDB/04046/2020 and UIDP/04046/2020 Centre grants from FCT (BioISI), FCT research project INTERPHENO (PTDC/ASP-PLA/28726/2017) is gratefully acknowledged. Pedro Correia acknowledges FCT (Portugal) for the financial support via a fellowship from the BioSys Ph.D. programme PD65-2012 (Ref SFRH/PD/BD/130973/2017). Thomas Roitsch would like to acknowledge support by the Ministry of Education, Youth and Sports of CR within the National Sustainability Pro-gram I (NPU I), grant number LO1415.

References

Albacete A, Cantero-Navarro E, Großkinsky DK, *et al.* 2015. Ectopic overexpression of the cell wall invertase gene CIN1 leads to dehydration avoidance in tomato. Journal of Experimental Botany **66**, 863–878.

Albacete AA, Großkinsky DK, Roitsch T. 2011. Trick and treat: a review on the function and regulation of plant invertases in the abiotic stress response.

Antonio Cuesta-Seijo J, De Porcellinis AJ, Valente AH, *et al.* 2019. Amylopectin Chain Length Dynamics and Activity Signatures of Key Carbon Metabolic Enzymes Highlight Early Maturation as Culprit for Yield Reduction of Barley Endosperm Starch after Heat Stress. Plant and Cell Physiology **60**, 2692–2706.

Araus JL. 2002. Plant Breeding and Drought in C3 Cereals: What Should We Breed For? Annals of Botany **89**, 925–940.

Blackburn GA. 2007. Hyperspectral remote sensing of plant pigments. Journal of Experimental Botany **58**, 855–867.

Bouslama M, Schapaugh WT. 1984. Stress Tolerance in Soybeans. I. Evaluation of Three Screening Techniques for Heat and Drought Tolerance 1 . Crop Science **24**, 933–937.

Bradford MM. 1976. A rapid and sensitive method for the quantitation of microgram quantities of protein utilizing the principle of protein-dye binding. Analytical Biochemistry **72**, 248–254.

Carmo-Silva AE, Gore MA, Andrade-Sanchez P, French AN, Hunsaker DJ, Salvucci ME. 2012. Decreased CO 2 availability and inactivation of Rubisco limit photosynthesis in cotton plants under heat and drought stress in the field. Environmental and Experimental Botany **83**, 1–11.

Catchpole WR, Wheeler CJ. 1992. Estimating plant biomass: A review of techniques. Austral Ecology **17**, 121–131.

Chaves MM, Maroco JP, Pereira JS. 2003. Understanding plant responses to drought — from genes to the whole plant. Functional Plant Biology **30**, 239.

Chen D, Fu LY, Hu D, Klukas C, Chen M, Kaufmann K. 2018*a*. The HTPmod Shiny application enables modeling and visualization of large-scale biological data. Communications Biology **1**, 1–8.

Chen D, Neumann K, Friedel S, Kilian B, Chen M, Altmann T, Klukas C. 2014. Dissecting the phenotypic components of crop plant growthand drought responses based on high-throughput image analysis w open. Plant Cell **26**, 4636–4655.

Chen D, Shi R, Pape JM, Neumann K, Arend D, Graner A, Chen M, Klukas C. 2018*b*. Predicting plant biomass accumulation from image-derived parameters. GigaScience **7**, 1–13.

Cobb JN, DeClerck G, Greenberg A, Clark R, McCouch S. 2013. Next-generation phenotyping: Requirements and strategies for enhancing our understanding of genotype-phenotype relationships and its relevance to crop improvement. Theoretical and Applied Genetics **126**, 867–887.

Correia PMP, Silva AB, Roitsch T, Carmo-Silva E, Marques da Silva J. 2021. Photoprotection and optimization of sucrose usage contribute to faster recovery of photosynthesis after water deficit at high temperatures in wheat. Physiologia Plantarum **172**, 615–628.

Costa JM, Grant OM, Chaves MM. 2013. Thermography to explore plant-environment interactions. Journal of Experimental Botany **64**, 3937–3949.

Deryng D, Conway D, Ramankutty N, Price J, Warren R. 2014. Global crop yield response to extreme heat stress under multiple climate change futures. Environmental Research Letters **9**, 034011.

Duque AS, de Almeida AM, Bernardes da Silva A, Marques da Silva J, Farinha AP, Santos D, Fevereiro P, Sousa Araujo S de. 2013. Abiotic Stress Responses in Plants: Unraveling the Complexity of Genes and Networks to Survive. Abiotic Stress - Plant Responses and Applications in Agriculture. InTech, .

Fahlgren N, Gehan MA, Baxter I. 2015. Lights, camera, action: High-throughput plant phenotyping is ready for a close-up. Current Opinion in Plant Biology **24**, 93–99.

FAOSTAT. 2019. *Food and Agriculture Organization of the United Nations*. Rome.

Fimognari L, Dölker R, Kaselyte G, Jensen CNG, Akhtar SS, Großkinsky DK, Roitsch T. 2020. Simple semi-high throughput determination of activity signatures of key antioxidant enzymes for physiological phenotyping. Plant Methods **16**, 42.

Fiorani F, Schurr U. 2013. Future Scenarios for Plant Phenotyping. Annual Review of Plant Biology **64**, 267–291.

Fischer RA, Maurer R. 1978. Drought resistance in spring wheat cultivars. I. Grain yield responses. Australian Journal of Agricultural Research **29**, 897–912.

Foyer CH, Noctor G. 2005. Oxidant and antioxidant signalling in plants: A re-evaluation of the concept of oxidative stress in a physiological context. Plant, Cell and Environment **28**, 1056–1071.

Giusti MM, Wrolstad RE. 2001. Characterization and Measurement of Anthocyanins by UV-Visible Spectroscopy. Current Protocols in Food Analytical Chemistry **00**.

Grubbs FE. 1950. Sample Criteria for Testing Outlying Observations. The Annals of Mathematical Statistics **21**, 27–58.

Grzesiak MT, Marcińska I, Janowiak F, Rzepka A, Hura T. 2012. The relationship between seedling growth and grain yield under drought conditions in maize and triticale genotypes. Acta Physiologiae Plantarum **34**, 1757–1764.

El Habti A, Fleury D, Jewell N, Garnett T, Tricker PJ. 2020. Tolerance of Combined Drought and Heat Stress Is Associated With Transpiration Maintenance and Water Soluble Carbohydrates in Wheat Grains. Frontiers in Plant Science **11**, 1555.

Jammer A, Gasperl A, Luschin-Ebengreuth N, *et al.* 2015. Simple and robust determination of the activity signature of key carbohydrate metabolism enzymes for physiological phenotyping in model and crop plants. Journal of Experimental Botany **66**, 5531–5542.

Junker A, Muraya MM, Weigelt-Fischer K, Arana-Ceballos F, Klukas C, Melchinger AE, Meyer RC, Riewe D, Altmann T. 2015. Optimizing experimental procedures for quantitative evaluation of crop plant performance in high throughput phenotyping systems. Frontiers in Plant Science **5**, 1–21.

Koussevitzky S, Suzuki N, Huntington S, Armijo L, Sha W, Cortes D, Shulaev V, Mittler R. 2008. Ascorbate peroxidase 1 plays a key role in the response of Arabidopsis thaliana to stress combination. Journal of Biological Chemistry **283**, 34197–34203.

Kuhn M. 2008. Building Predictive Models in R Using the caret Package. Journal of Statistical Software; Vol 1, Issue 5 (2008) .

Lascano HR, Antonicelli GE, Luna CM, Melchiorre MN, Gómez LD, Racca RW, Trippi VS, Casano LM. 2001. Antioxidant system response of different wheat cultivars under drought: Field and in vitro studies. Australian Journal of Plant Physiology **28**, 1095–1102.

Lawson T, Terashima I, Fujita T, Wang Y. 2018. Coordination Between Photosynthesis and Stomatal Behavior.141–161.

Louis Joosen RV, Arends D, Li Y, Willems LAJ, Keurentjes JJB, Ligterink W, Jansen RC, Hilhorst HWM. 2013. Identifying genotype-by-environment interactions in the metabolism of germinating arabidopsis seeds using generalized genetical genomics. Plant Physiology **162**, 553–566.

Manès Y, Gomez HF, Puhl L, Reynolds M, Braun HJ, Trethowan R. 2012. Genetic yield gains of the CIMMYT International semi-arid wheat yield trials from 1994 to 2010. Crop Science **52**, 1543–1552.

Meade KA, Cooper M, Beavis WD. 2013. Modeling biomass accumulation in maize kernels. Field Crops Research **151**, 92–100.

Merzlyak MN, Gitelson AA, Chivkunova OB, Solovchenko AE, Pogosyan SI. 2003. Application of Reflectance Spectroscopy for Analysis of Higher Plant Pigments. Russian Journal of Plant Physiology **50**, 704–710.

Moore G. 2015. Strategic pre-breeding for wheat improvement. Nature Plants **1**.

Moore B, Zhou L, Rolland F, Hall Q, Cheng WH, Liu YX, Hwang I, Jones T, Sheen J. 2003. Role of the Arabidopsis glucose sensor HXK1 in nutrient, light, and hormonal signaling. Science **300**, 332–336.

Moshelion M. 2020. The dichotomy of yield and drought resistance. EMBO reports **21**, e51598.

Nunes C, Araújo S., Silva JM, Fevereiro P, Silva AB. 2009. Photosynthesis light curves: a method for screening water deficit resistance in the model legume *Medicago truncatula*. Annals of Applied Biology **155**, 321–332.

Paine CET, Marthews TR, Vogt DR, Purves D, Rees M, Hector A, Turnbull LA. 2012. How to fit nonlinear plant growth models and calculate growth rates: An update for ecologists. Methods in Ecology and Evolution **3**, 245–256.

Parent B, Bonneau J, Maphosa L, Kovalchuk A, Langridge P, Fleury D. 2017. Quantifying wheat sensitivities to environmental constraints to dissect genotype × environment interactions in the field. Plant Physiology **174**, 1669–1682.

Pennacchi JP, Carmo-Silva E, Andralojc PJ, Lawson T, Allen AM, Raines CA, Parry MAJ. 2019. Stability of wheat grain yields over three field seasons in the UK. Food and Energy Security **8**, e00147.

Pinheiro C, Chaves MM. 2011. Photosynthesis and drought: Can we make metabolic connections from available data? Journal of Experimental Botany **62**, 869–882.

Reynolds MP, Pask AJD, Hoppitt WJE, *et al.* 2017. Strategic crossing of biomass and harvest index—source and sink—achieves genetic gains in wheat. Euphytica **213**, 257.

Reynolds MP, Pierre C Saint, Saad ASI, Vargas M, Condon AG. 2007. Evaluating Potential Genetic Gains in Wheat Associated with Stress-Adaptive Trait Expression in Elite Genetic Resources under Drought and Heat Stress. Crop Science **47**.

Rizhsky L, Liang H, Shuman J, Shulaev V, Davletova S, Mittler R. 2004. When defense pathways collide. The response of arabidopsis to a combination of drought and heat stress 1[w]. Plant Physiology **134**, 1683–1696.

Rohart F, Gautier B, Singh A, Lê Cao K-A. 2017. mixOmics: An R package for 'omics feature selection and multiple data integration (D Schneidman, Ed.). PLOS Computational Biology **13**, e1005752.

Roitsch T, Cabrera-Bosquet L, Fournier A, Ghamkhar K, Jiménez-Berni J, Pinto F, Ober ES. 2019. Review: New sensors and data-driven approaches—A path to next generation phenomics. Plant Science **282**, 2–10.

Roitsch T, González MC. 2004. Function and regulation of plant invertases: Sweet sensations. Trends in

Plant Science **9**, 606–613.

Russo S, Sillmann J, Fischer - EM, Krysanova V, Vetter T, Eisner S, - al. 2018. Environmental Research Letters Future heat-waves, droughts and floods in 571 European cities Related content Top ten European heatwaves since 1950 and their occurrence in the coming decades Anthropogenic climate change affects meteorological drought risk in Europe L Gudmundsson and S I Seneviratne-Intercomparison of regional-scale hydrological models and climate change impacts projected for 12 large river basins worldwide-a synthesis This content was downloaded from IP address. **18**, 15.

Sairam RK, Srivastava GC, Saxena DC. 2000. Increased antioxidant activity under elevated temperatures: A mechanism of heat stress tolerance in wheat genotypes. Biologia Plantarum **43**, 245–251.

Secchi F, Zwieniecki MA. 2016. Accumulation of sugars in the xylem apoplast observed under water stress conditions is controlled by xylem pH. Plant Cell and Environment **39**, 2350–2360.

Seelig HD, Hoehn A, Stodieck LS, Klaus DM, Adams WW, Emery WJ. 2008. The assessment of leaf water content using leaf reflectance ratios in the visible, near-, and short-wave-infrared. International Journal of Remote Sensing **29**, 3701–3713.

Shokat S, Großkinsky DK, Roitsch T, Liu F. Activity of leaf and spike carbohydrate-metabolic and antioxidant enzymes linked with yield performance in three spring wheat genotypes grown under well-watered and drought conditions.

Shokat S, Großkinsky DK, Roitsch T, Liu F. 2020. Activities of leaf and spike carbohydrate-metabolic and antioxidant enzymes are linked with yield performance in three spring wheat genotypes grown under well-watered and drought conditions. BMC Plant Biology **20**, 400.

Singleton VL, Orthofer R, Lamuela-Raventós RM. 1999. Analysis of total phenols and other oxidation substrates and antioxidants by means of folin-ciocalteu reagent. Methods in Enzymology **299**, 152–178.

Stekhoven DJ, Bühlmann P. 2012. Missforest-Non-parametric missing value imputation for mixed-type data. Bioinformatics **28**, 112–118.

Tardieu F. 2012. Any trait or trait-related allele can confer drought tolerance: Just design the right drought scenario. Journal of Experimental Botany **63**, 25–31.

Tardieu F, Cabrera-Bosquet L, Pridmore T, Bennett M. 2017. Plant Phenomics, From Sensors to Knowledge. Current biology : CB **27**, R770–R783.

Tessmer OL, Jiao Y, Cruz JA, Kramer DM, Chen J. 2013. Functional approach to high-throughput plant growth analysis. BMC Systems Biology **7**, 1–13.

Tricker PJ, Elhabti A, Schmidt J, Fleury D. 2018. The physiological and genetic basis of combined

drought and heat tolerance in wheat. Journal of Experimental Botany **69**, 3195–3210.

Whittaker A, Bochicchio A, Vazzana C, Lindsey G, Farrant J. 2001. Changes in leaf hexokinase activity and metabolite levels in response to drying in the desiccation-tolerant species Sporobolus stapfianus and Xerophyta viscosa. Journal of Experimental Botany **52**, 961–969.

Woodward FI, Hunt R. 1983. Plant Growth Curves: The Functional Approach to Plant Growth Analysis. The Journal of Applied Ecology **20**, 695.

Zampieri M, Ceglar A, Dentener F, Toreti A. 2017. Wheat yield loss attributable to heat waves, drought and water excess at the global, national and subnational scales. Environmental Research Letters **12**.

Zandalinas SI, Balfagón D, Arbona V, Gómez-Cadenas A. 2017. Modulation of Antioxidant Defense System Is Associated with Combined Drought and Heat Stress Tolerance in Citrus. Frontiers in Plant Science **8**, 953.

Zhang G, Zhang M, Zhao Z, Ren Y, Li Q, Wang W. 2017. Wheat TaPUB1 modulates plant drought stress resistance by improving antioxidant capability. Scientific Reports **7**, 1–13.

Zhishen J, Mengcheng T, Jianming W. 1999. The determination of flavonoid contents in mulberry and their scavenging effects on superoxide radicals. Food Chemistry **64**, 555–559.

Figures and tables

Table 1 – List of the ten wheat genotypes used in this study.

GenotypeID*	Cross Name	Information	GID CIMMYT	Source (tested)
PASTOR	W15.92/4/PASTOR//HXL7573/2*BAU/3/WBLL1	PT Line	5865676	CIMMYT (7^{th} SATYN)
SOKWB_1	SOKOLL/WBLL1	PT Line	6056139	CIMMYT (7^{th} SATYN)
BORLAUG100	BORLAUG100 F2014	Check	7806808	CIMMYT (7^{th}, 8^{th} SATYN)
CMH82	CMH82.575/CMH82.801	Parental	1187021	CIMMYT (Reynolds *et al.*, 2007)
PUBWB	PUB94.15.1.12/WBLL1	PT Line	6056064	CIMMYT (8^{th} SATYN)
SOKWB_2	SOKOLL/WBLL1	PT Line	6056140	CIMMYT (8^{th} SATYN)
SOKOLL	SOKOLL	Check Parental	3825355	CIMMYT (7^{th}, 8^{th} SATYN)
KSPA	KS940935.7.1.2/2*PASTOR	Parental	5865910	CIMMYT (Manès *et al.*, 2012)
BAJ	BAJ #1	Check	5106304	CIMMYT (7^{th}, 8^{th} SATYN)
PARAGON	CSW1724-19-5-68//Axona/Tonic	UK elite line	NA	LEC, UK (Correia *et al.*, 2021)

* ID adopted for this study based on the cross name simplification

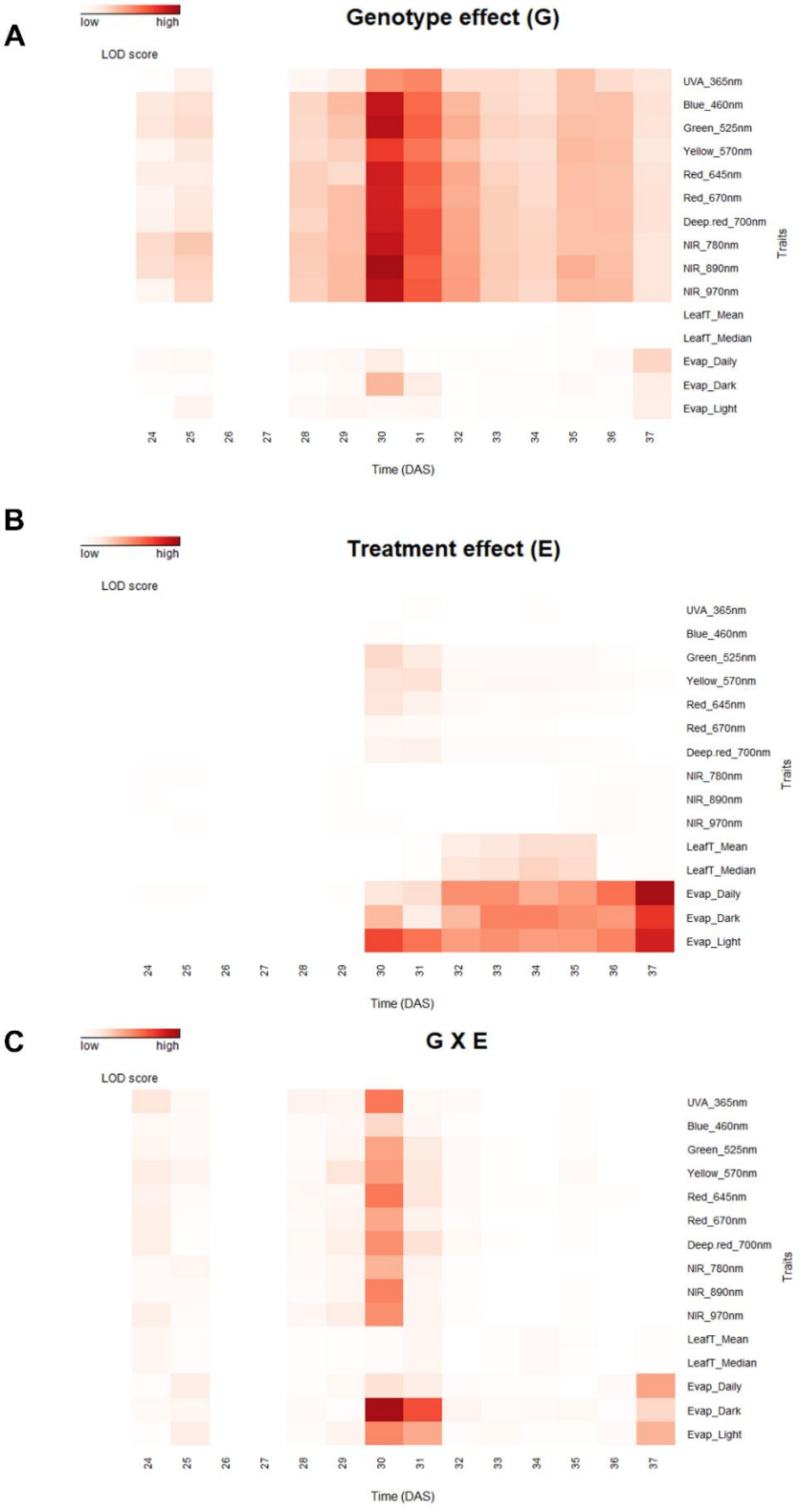

Figure 1 – Phenotypic variation over-time of wheat plants exposed to high temperature (WW38) or water deficit at high temperature (WD38). (A) Statistical significance of genotype effect, **(B)** treatment effect (WW38 vs WD38), and **(C)** their interaction effect (GxE) for each phenotype trait measured in each day. The shading plot indicates the significance level (Bonferroni corrected P values) in LOD scores (-log probability). There is no difference between the groups' means in white cells, and different shades of red indicate the strength of the significant difference between groups.

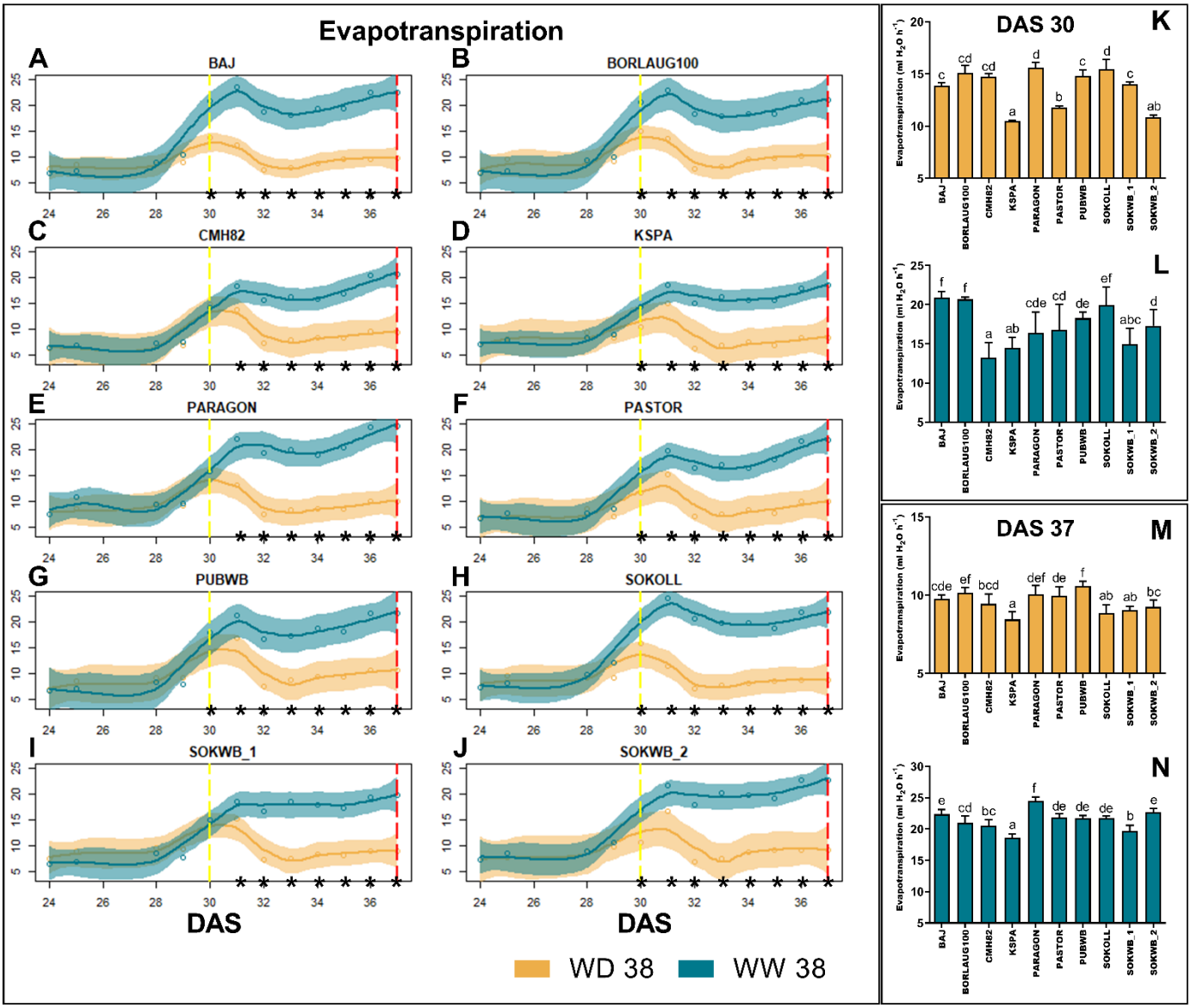

Figure 2 – Evapotranspiration over-time of wheat plants exposed to high temperature (WW38) or water deficit at high temperature (WD38). (A-J) Measurements were taken continuously throughout the experiment for each genotype in plants under WW38 and WD38. **(K,L)** Comparison of genotypes at the start of the stress imposition (30 DAS). **(M,N)** Comparison of genotypes at the end of the experiment (37 DAS). Blue lines and bars represent WW38 plants; yellow solid lines and bars represent WD38 plants. Shaded areas represent 95% confidence intervals. Yellow dashed lines denote stress imposition (30 DAS) and red dashed lines the end of the experiment (37 DAS). Asterisks denote significant differences between treatments in each genotype (t-test, $P<0.05$, A-J). Bar charts show mean values ± SEM (n = 5 biological replicates). Different letters denote significant differences between genotypes (Duncan analysis, $P<0.05$).

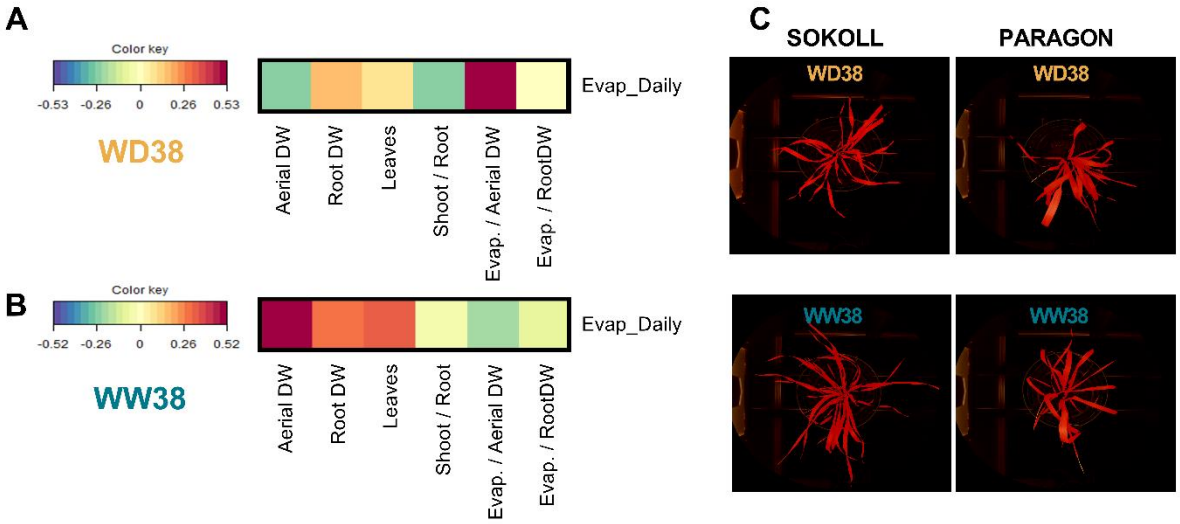

Figure 3 – Relative importance of biomass and architecture traits to evapotranspiration at DAS 37 of wheat plants exposed to water deficit at high temperature (WD38, A) or high temperature (WW38, B). Heatmap represents a correlation between evapotranspiration and traits related to biomass and plants architecture. Evap: evapotranspiration; Evap/RootDW: evapotranspiration normalized to root dry biomass; Evap/AerialDW: evapotranspiration normalized to aboveground dry biomass; Shoot/Root: shoot to root mass fraction (Fig. S2); Leaves: number of leaves per plant (Fig. S2), Root DW: roots dry biomass; Aerial DW: aboveground dry biomass. **(C)** Representative images of architectural differences between genotypes, segmented images of SOKOLL and PARAGON. The leaves are shown in red.

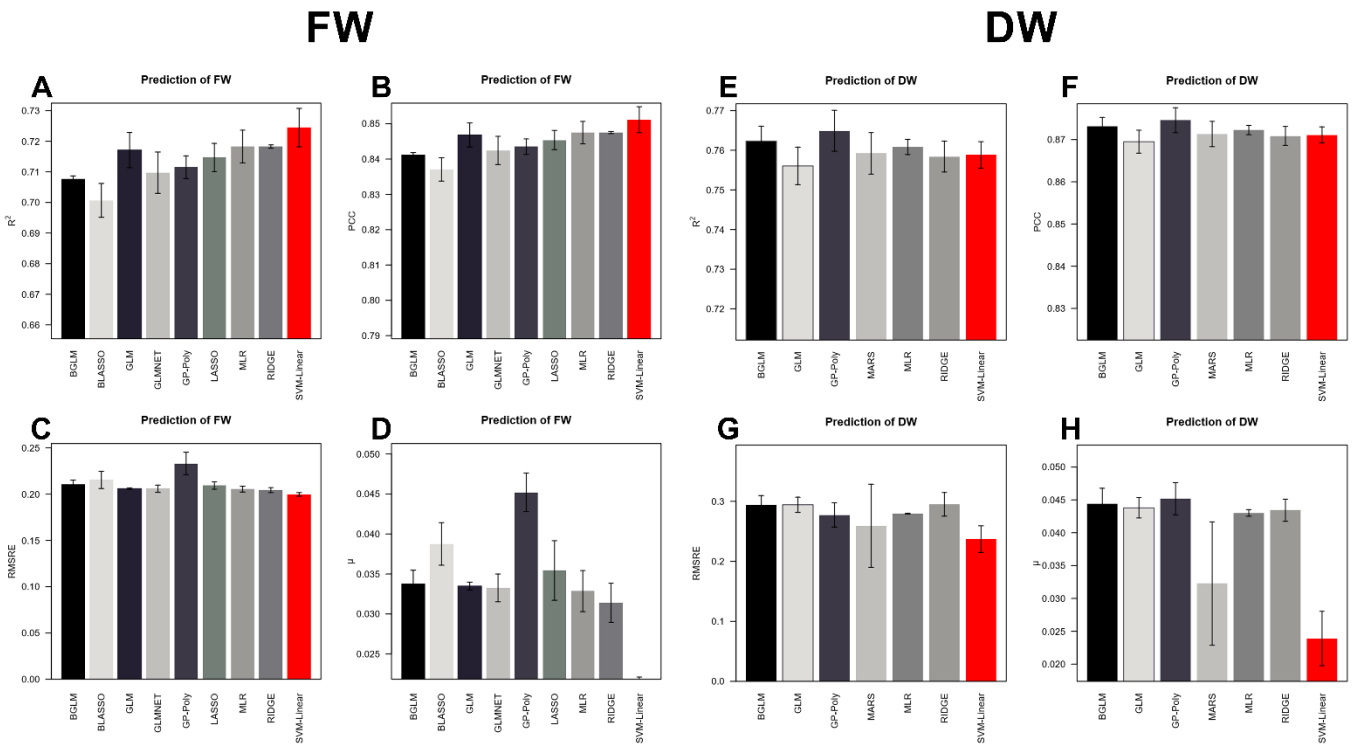

Figure 4 – Performance of nine machine-learning regression models considered for predicting plant biomass (FW, A-D, and DW, E-H) by image-extracted parameters (37 DAS). Models: (1) BGLM: Bayesian Generalized Linear Model; (2) BLASSO: Bayesian Lasso; (3) GLM: Generalized Linear Model; (4) GLMNET: Lasso and Elastic-Net Regularized Generalized Linear Models; (5) GP-Poly: Gaussian Process with Polynomial Kernel; (6) LASSO: Lasso Model; (7) MLR: Multivariate Linear Regression; (8) RIDGE: Ridge Regression; (9) SVM-Linear: Support Vector Machines with Linear Kernel. (**A**, **E**) R^2: Pearson correlation coefficient of determination between the predicted values and the observed values ; (**B**,**F**) PCC: Pearson correlation coefficient; (**C**,**G**) MRSR: root mean squared relative error of cross-validation; (**D**,**H**) *μ:* predictive bias between the predicted and observed values.

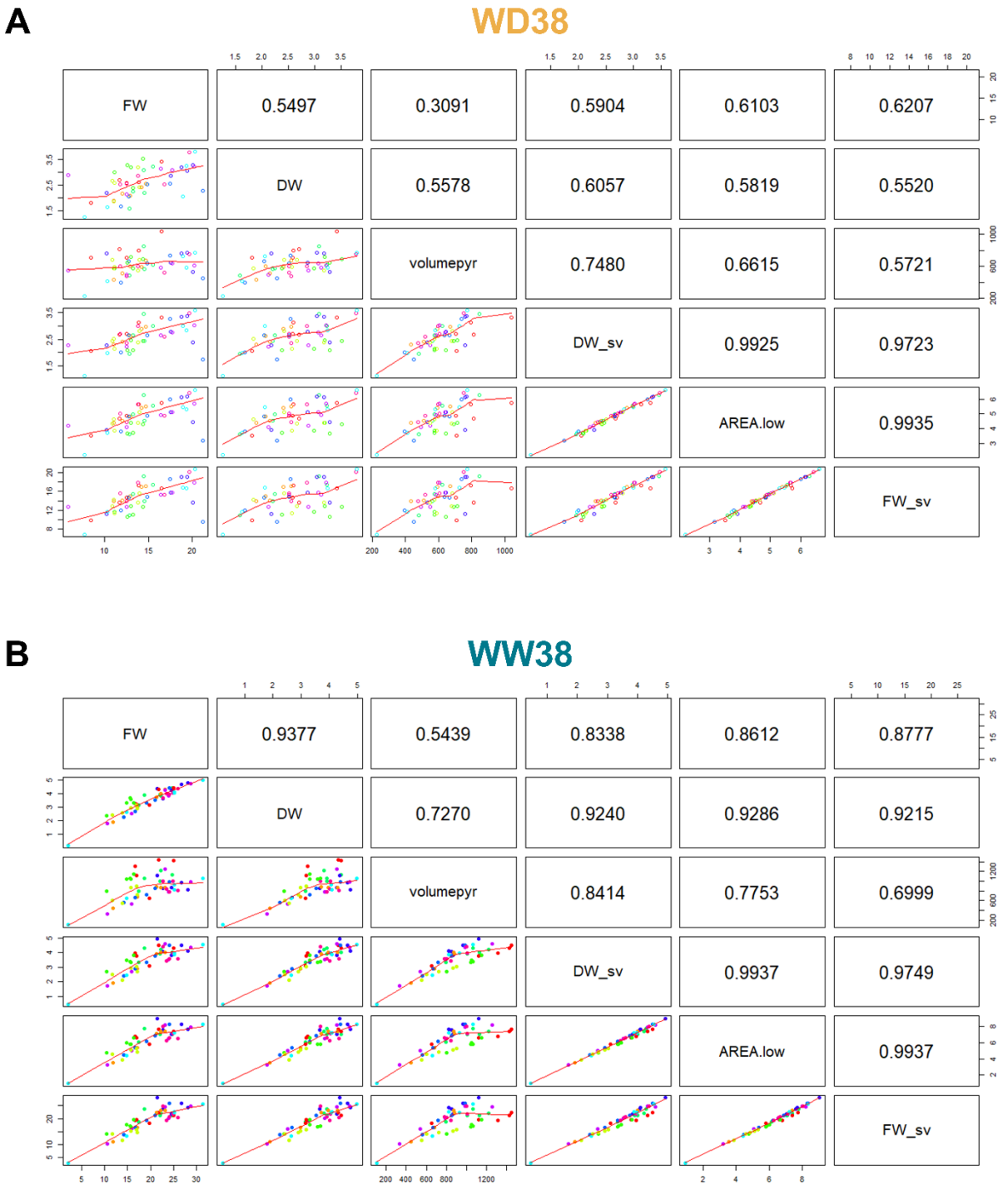

Figure 5 – Pearson correlation matrix between manual measurements, image-derived features, and model-predicted data from plants growing at WD38 (A) and WW38 (B). Values are correlation coefficients (r). FW: aboveground fresh biomass; DW: aboveground dry biomass; FW_sv: predicted fresh biomass (SVM-linear); DW_sv: predicted dry biomass (SVM-linear); AREA.low: exposed leaf area extracted from images; volumepyr: plant pyramidal volume calculated based on image-derived features. Different coloured dots represent genotypes.

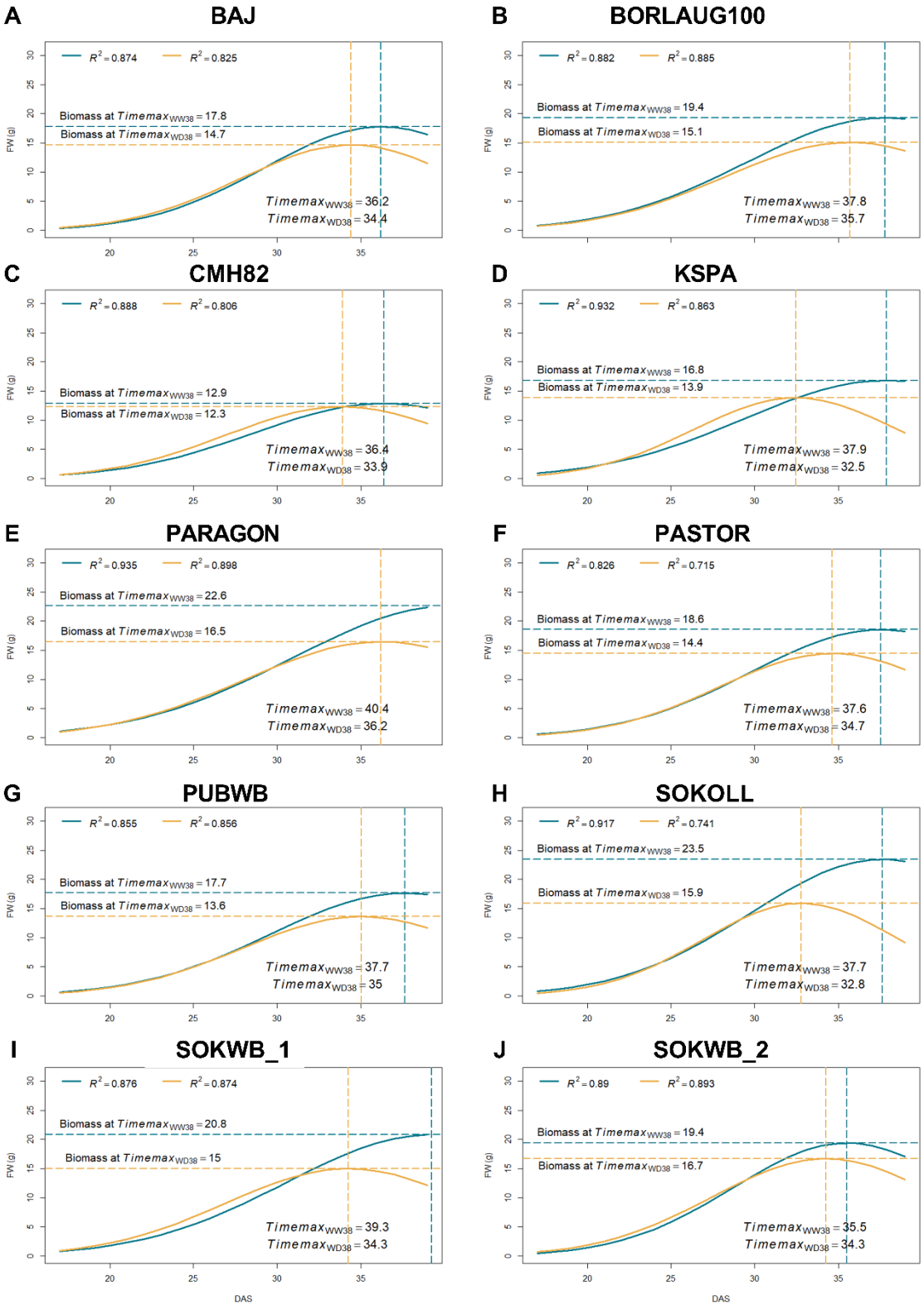

Figure 6 – Modelling plant growth in ten wheat genotypes exposed to high temperature (WW38) or water deficit at high temperature (WD38). Growth models are based on fitting predicted biomass values from 24 to 41 DAS using a bell shape model. Blue lines represent WW38 plants and yellow lines represent WD38 plants. Quality of fit (R^2) of each model, the time point of maximum biomass (Timemax, vertical dashed lines) and maximum growth capacity (Biomass at Timemax, horizontal dashed lines) are indicated.

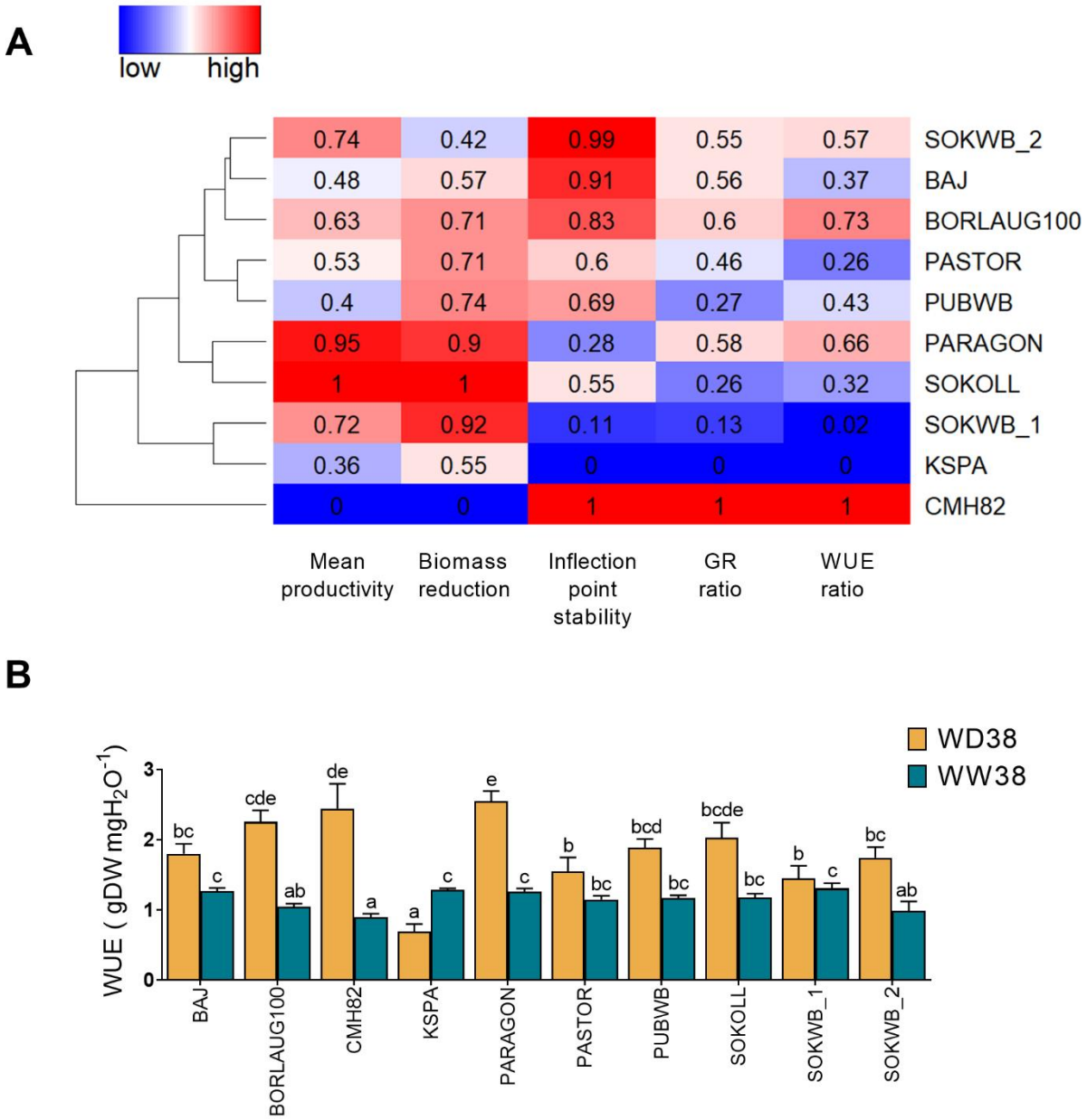

Figure 7 – Stress tolerance indices of ten wheat genotypes when exposed to high temperature (WW38) or water deficit at high temperature (WD38). (A) Heat map representation of rescaled values (0-1) of Mean productivity, Biomass reduction, Inflection point stability, growth rate (GR) and water use efficiency (WUE) ratios of WD38 to WW38. Blue cells represent low values and red cells high values. Hierarchical clustering was applied to the matrix rows. **(B)** Water use efficiency, as biomass produced per water transpiration. Different letters denote statistically significant differences between genotypes (Duncan analysis, $P<0.05$. Mean productivity = (Biomass at $Timemax_{WW38}$ + Biomass at $Timemax_{WD38}$)/2; Biomass reduction = Biomass at $Timemax_{WD38}$ / Biomass at $Timemax_{WW38}$; Inflection point stability = $Timemax_{WW38}-Timemax_{WD38}$; GR ratio=$GR_{WD38}$ / GR_{WW38}; WUE ratio=WUE_{WD38} /WUE_{WW38}.

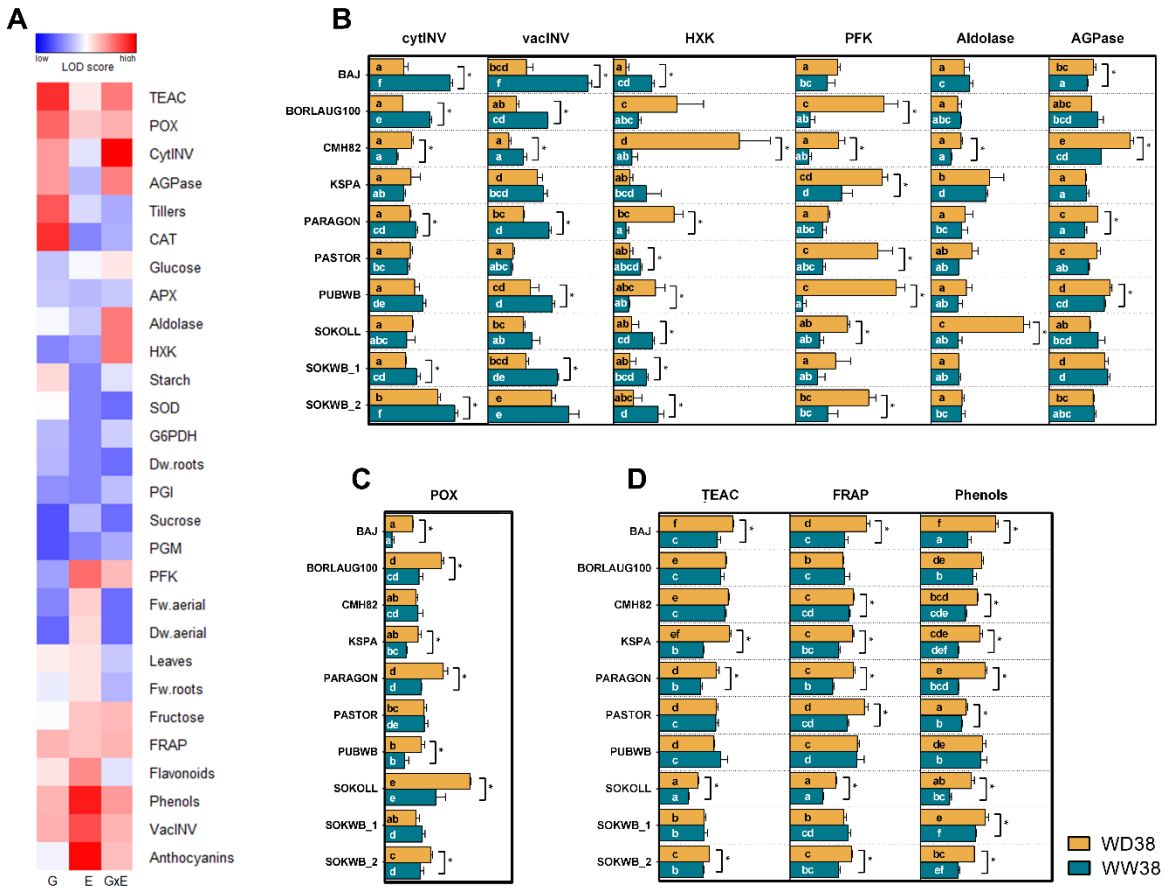

Figure 8 – Adjustments of the carbohydrate and antioxidant metabolisms of wheat when exposed to high temperature (WW38) or water deficit at high temperature (WD38). (A) Statistical significance of genotype effect, treatment effect (WW38 vs WD38), and their interaction (GxE) for each trait measured at the end of the experiment (37 DAS). The shading plot indicates the significance level (Bonferroni corrected P values) in LOD scores (-log probability). Blue cells represent low LOD values and red cells high values. **(B-C)** Top 10 traits with highest GxE LOD scores. **(B)** Carbohydrate metabolism enzymes activity expressed relative to the amount of TSP. **(C)** Peroxidase activity expressed relative to the amount of TSP. **(D)** Antioxidant capacities and total phenols (mg/g of equivalents). Asterisks denote significant differences between treatments in each genotype (t-test, *P*<0.05). Bars show mean values ± SEM (n = 4-5 biological replicates), and different letters denote statistically significant differences between genotypes (Duncan analysis, *P*<0.05).